Inherent multistability in arrays of autoinducer coupled genetic oscillators

A. Koseska,[1] E. Volkov,[2] A. Zaikin,[1,3] and J. Kurths[1]
[1]*Institut für Physik, Potsdam Universität, Am Neuen Palais 10, D-14469 Potsdam, Germany*
[2]*Department Theoretical Physics, Lebedev Physical Institute, Leninskii 53, Russia*
[3]*Department of Mathematics, University of Essex, Wivenhoe Park, Colchester C04 3SQ, United Kingdom*
(Received 4 December 2006; published 30 March 2007)

Rhythm generation mechanisms are very important for genetic network functions as well as for the design of synthetic genetic circuits. A significant attention to date has been focused on the synchronization of communicating genetic units, which results in the production of an unified rhythm. In contrast to this we address the question: what mechanisms of intercell communication can be responsible for multirhythmicity in globally coupled genetic units? Here, we show that an autoinducer intercell communication system that provides coupling between synthetic genetic oscillators will inherently lead to multirhythmicity and the appearance of several coexisting dynamical regimes, if the time evolution of the genetic network can be split in two well-separated time scales. We investigate in detail a variety of dynamical regimes in a genetic population and show the possibility for multiple element distributions between clusters, as well as the possibility of generating complex oscillations with different return times in one limit cycle.

DOI: 10.1103/PhysRevE.75.031916 PACS number(s): 87.18.−h, 05.40.Ca, 05.45.Xt, 87.15.Ya

I. INTRODUCTION

The ability to design and construct synthetic genetic regulatory networks provides a natural framework to study the dynamics of gene regulation. This also opens numerous applications in biotechnology, where a new approach is envisioned, e.g., in drug production or in the design of the new-era computing devices, based directly on synthetic genetic circuits [1]. Several rather simple genetic networks have been recently proposed and experimentally constructed, e.g., toggle switches [2], the repressilator [3], relaxator models [4,5], different logic circuits [6], etc.

Recently, the possibility to use the quorum sensing mechanism in order to investigate global synchronization in synthetic genetic networks has been reported for deterministic [5,7–9], as well as for noise-driven [10] genetic oscillators. It is important to point out that these genetic circuits function in arrays and mostly they operate coupled through small molecules of autoinducer (AI) diffusing between cells. This intercellular signaling mechanism in certain models [5,8] is governed by a slow time scale in the system and the coupling is organized through the slow recovery variable in the genetic network. As known from oscillation theory, such coupling has a phase-repulsive property and can be referred to as inhibitory. On the other hand, local coupling of limit cycles via inhibitory variables has been reported to yield a coexistence of different stable attractors [11–13], thus making the multirhythmicity in such systems rather typical. Note that increased relaxatory dynamics, i.e., enhanced separation of time scales, of the individual elements leads to increased parametric areas of individual stability for different periodic attractors, as well as increased hysteresis areas [14,15].

Multirhythmicity appearing due to the complex structure of isolated oscillators has been investigated by Decrloy and Goldbeter [16], or more recently in [17]. In contrast to this, multirhythmicity evoked by the interactions of general identical biological [18–20] or technical [21] oscillators is mainly a subject of recent investigations. Multirhythmicity has been also reported in earlier simulations of coupled circadian oscillators [22–24]. However, the mechanisms that lead to multirhythmicity in globally coupled genetic oscillators differ substantially from those reported for circadian oscillators. A main manifestation of multistability for systems of globally coupled oscillators is clustering, defined as a dynamical state of the system characterized with the coexistence of several subgroups, where the oscillators exhibit identical behavior. Clustering has been investigated for different systems, including identical one-dimensional maps, e.g., logistic or circle maps [25]. Regarding oscillators, the clustering has been proved theoretically for identical phase oscillators [26,27], observed experimentally for salt-water oscillators [28] or electrochemical oscillators [29,30], etc. However, multirhythmicity and coexistence of several attractors, well known for abstract mathematical models, have not been reported for concrete genetic networks. These effects can be very important for the construction of genetic networks and understanding of evolutionary mechanisms behind the cell differentiation and genetic clock functioning. The ability of a genetic unit to produce different dynamical regimes which coexist also means its improved adaptability: if one of the regimes becomes unprofitable for cell functioning, the genetic unit can easily switch to some of the other coexisting regimes available. Moreover, coexistence of different regimes opens the possibility for construction of a "genetic-based" information storage devices.

In this paper we show that multirhythmicity is a typical property of genetic networks with multiple time scale dynamics and autoinducer intercell communication system. The subject of our study is, therefore, a model constructed from genetic networks previously investigated in separate experiments—the toggle switch coupled via the quorum sensing mechanism [8]. First, we present by direct calculations the existence of different dynamical regimes and clustering with different element distribution between clusters. Next, we give a detailed bifurcation analysis for a system of two coupled genetic oscillators, and show the richness of dynamical regimes and the parameter ranges in which these

regimes can be realized. Finally, we discuss the importance of these dynamical regimes in arrays of AI coupled genetic networks for new applications regarding the design of genetic clocks, synchronization properties with the cell cycle [4], chronotherapy, etc.

II. MODEL EQUATIONS

We consider a model of hysteresis-based relaxation genetic oscillators coupled via the quorum sensing mechanism, recently proposed in [8]. The oscillator is constructed by combining two engineered gene networks, the toggle switch [2] and an intercell communication system, which have been previously implemented experimentally in *Escherichia coli* [31] and *Vibrio fischeri* [32]. The synthesis of the two repressor proteins, which constitute the toggle switch, are regulated in such a way that the expression of the two genes is mutually exclusive, organizing bistability. The second network is based on the dynamics of an autoinducer, which on the one hand drives the toggle switch through the hysteresis loop, and on the other hand provides an intercell communication by diffusion through the cell membrane.

The time evolution of the elements in the system is governed by the dimensionless equations (see details in [8]):

$$\frac{du_i}{dt} = \alpha_1 f(v_i) - u_i + \alpha_3 h(w_i), \tag{1}$$

$$\frac{dv_i}{dt} = \alpha_2 g(u_i) - v_i, \tag{2}$$

$$\frac{dw_i}{dt} = \varepsilon[\alpha_4 g(u_i) - w_i] + 2d(w_e - w_i), \tag{3}$$

$$\frac{dw_e}{dt} = \frac{d_e}{N}\sum_{i=1}^{N}(w_i - w_e), \tag{4}$$

where N is the total number of cells (oscillators), u_i and v_i represent the proteins from which the toggle switch is constructed in the ith cell, and w_i represents the intracellular and w_e the extracellular AI concentration (Fig. 1). The mutual influence of the genes is defined with the functions

$$f(v) = \frac{1}{1+v^{\beta}}, \quad g(u) = \frac{1}{1+u^{\gamma}}, \quad h(w) = \frac{w^{\eta}}{1+w^{\eta}},$$

where β, η, and γ are the parameters of the corresponding activatory or inhibitory Hill functions.

In Eqs. (1) and (2), the dimensionless parameters α_1 and α_2 regulate the repressor operation in the toggle switch, α_3, the activation due to the AI, and α_4 the repressing of the AI. The coupling coefficients in the system are given by d and d_e (intracellular and extracellular) and depend mainly on the diffusion properties of the membrane, as well as on the ratio between the volume of the cells and the extracellular volume [8]. If the parameter ε is small ($\varepsilon \ll 1$) [8], as in our case, the evolution of the system splits into two well-separated time scales, a fast dynamics of u_i, v_i and a slow dynamics of w_i. Due to this presence of multiple time scales, the system can produce relaxation oscillations.

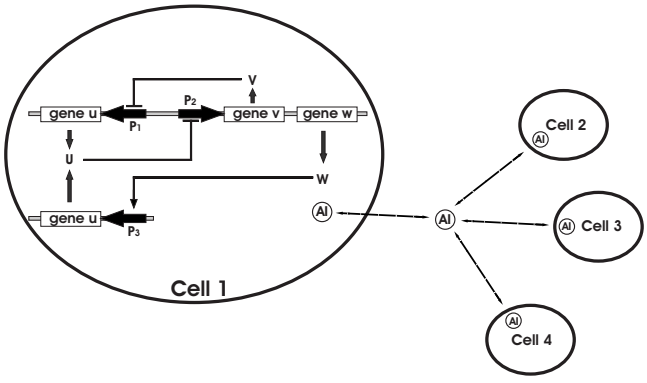

FIG. 1. Schematic diagram of the network of genetic relaxation oscillators. u, v, and w denote the genes, and P_1, P_2, and P_3 the corresponding promoters. AI refers to the autoinducer molecules.

III. MULTISTABILITY AND CLUSTERIZATION

Contemporary models of synthetic genetic oscillators coupled with AI exchange exhibit mainly in-phase oscillatory behavior [5,7,8]. Additionally, oscillation death (OD) in synthetic genetic oscillators has been discussed [8]. However, the appearance of other regimes or clustering, as well as the possibility for different distributions between clusters has not been observed in synthetic genetic networks. We report here the presence of multirhythmicity and clustering by means of numerical simulations for a system of globally coupled relaxation synthetic genetic oscillators. It is important to note that all of the solutions presented in this paper can be obtained for any network size. Two main phenomena are discussed here. First, we show the existence of different possible modes of organized collective behavior in the system of globally coupled relaxation genetic oscillators. We distinguish between two different types of clusters: (i) steady state clusters (Fig. 2) and (ii) oscillatory clusters (Fig. 3). Second, for each separate cluster formation, we demonstrate how the dependence on initial conditions can lead to different distributions of the oscillators between the clusters. In general, a system consisting of N oscillators can exhibit $N-1$ different distributions of the oscillators among the clusters.

(i) Oscillation death, called also inhomogeneous steady states, was initially discovered by Prigogine and Lefever [33] in a system of two coupled Brusselators. Furthermore, Bar-Eli [34] showed that OD persists in a large region of parameters in several models of diffusively coupled chemical oscillators. Extensive numerical and experimental investigations of OD for globally coupled systems have been presented for electrochemical oscillators [35]. However, clustering is not observed because a two-oscillator system was used. Recently, these phenomena have been reported for different biological system, such as two coupled β cells of the pancreatic islet of Langerhans [18].

The oscillators engaged in the OD regime in our model are distributed among two clusters and remain in a steady state, i.e., producing constant protein levels in the cell [Figs.

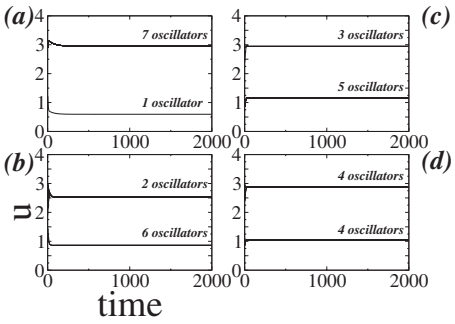

FIG. 2. Examples of different distributions in the steady state clusters for the system (1)–(4) with $N=8$ oscillators. Parameters: $\varepsilon=0.01$, $\alpha_1=3$, $\alpha_2=5$, $\alpha_3=1$, $\alpha_4=4$, $\beta=\eta=\gamma=2$, $d=0.3$, and $d_e=1$. Distribution (a) 1:7, where seven oscillators occupy the higher level; (b) 2:6; (c) 3:5; and (d) 4:4. Note the different protein levels for different oscillator distributions.

2(a)–2(d)]. We have found the existence of $(N-1)$ possible different distributions of the oscillators between these two clusters, each characterized by a shift in the protein production level. Examples of different distributions are plotted in Figs. 2(a)–2(d).

(ii) When the cells are identical, the coupled system is symmetric and identical behavior of the cells in the system is always a solution, though not necessarily a stable one [Fig. 3(a)]. However, the inhibitory coupling and the presence of multiple time scales, as previously discussed, create the possibility for multistability and multirhythmicity, resulting in the generation of various dynamical regimes. It is important to note that the dependence of the regime formation on the value of the coupling coefficient d gives rise to the formation of oscillatory clusters. When referring to oscillatory clusters, we speak about a cluster state characterized by the coexistence of subgroups, each of them containing in-phase-synchronized oscillations. For $d<0.01$, the system can exhibit antiphase oscillations, with oscillators distributed between the two oscillatory clusters [Figs. 3(b) and 3(c)]. An important feature to be mentioned is the characterization of different distributions with different periods of the limit cycle, providing more complex dynamics with different rhythms [compare Fig. 3(b) (5:3 distribution) with period $T=364.15$ and Fig. 3(c) (4:4 distribution) with period $T=256.27$].

Another mode of possible collective behavior of this system is asymmetric oscillations (for $d<0.003$), when some of the oscillators in the system perform large excursions, while the rest oscillate in the vicinity of a stable steady state with small amplitude. This results in the presence of two oscillatory clusters [Figs. 3(d) and 3(e)]. Again, the number of possible different distributions for a system of N oscillators is $(N-1)$, and each has a different period of oscillations [compare Fig. 3(d) (1:7) with period $T=216.95$ and Fig. 3(e) (4:4) with $T=141.01$].

The oscillators in the system can be also ordered in multiple cluster regimes; we present only two examples here, three [Fig. 3(f)] and five [Fig. 3(g)] oscillatory clusters. Again, different distributions of the oscillators between the clusters are possible in this case. To illustrate this, we present

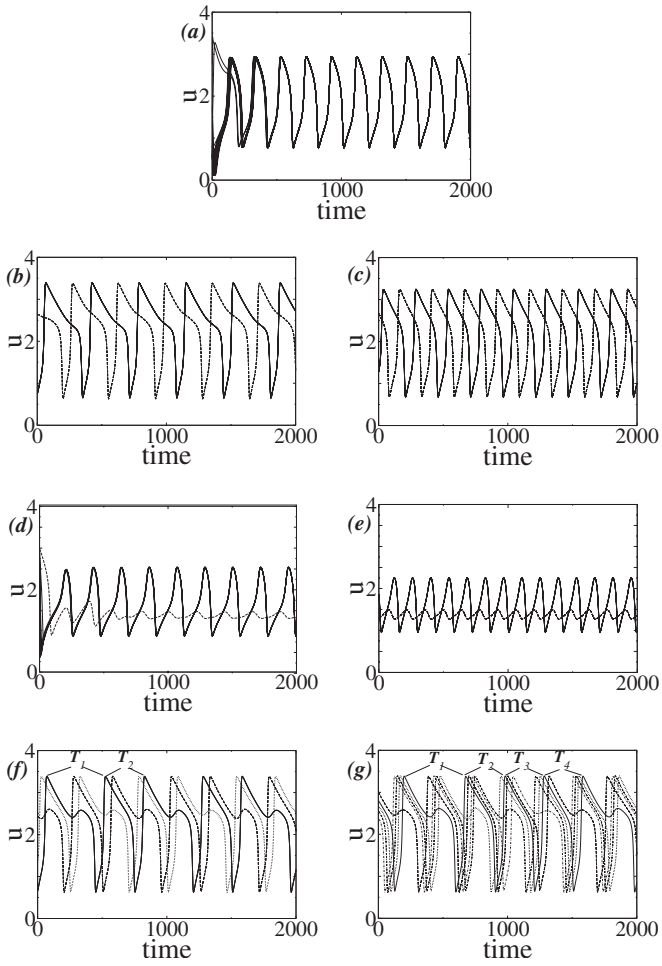

FIG. 3. Different oscillatory clusters for system of $N=8$ oscillators. (a) In-phase oscillations, $\alpha_1=3$, $d=0.005$; (b),(c) antiphase oscillations with different distributions of the oscillators between clusters, $\alpha_1=3.3$, $d=0.001$; (d),(e) asymmetric solution with different distribution of the oscillators: $\alpha_1=2.868$, $d=0.001$; (f) three oscillatory clusters $\alpha_1=3.3$, $d=0.001\,05$; and (g) five oscillatory clusters $\alpha_1=3.3$, $d=0.001$. For other parameters see Fig. 2.

here a 3:3:2 distribution when three oscillatory clusters are formed [Fig. 3(f)], and a 1:2:2:2:1 distribution when five oscillatory clusters are created [Fig. 3(g)]. In these multiple oscillatory cluster regimes, the cycles may contain several subcycles, an effect previously not observed in genetic networks and stable in certain parametric spaces. The complexity of these oscillatory regimes manifests itself through the generation of different return times in one limit cycle, and could have further impact on biotechnological applications, since it enables the possibility of synchronization properties with an external cycle (e.g., the cell cycle) in a broader frequency range.

IV. IDENTIFICATION OF DYNAMICAL REGIMES THROUGH A BIFURCATION ANALYSIS

Since the dynamics of the toggle switch and hence of the whole system is determined mainly by the parameters α_1 and α_2, we choose α_1 as a bifurcation parameter and study more

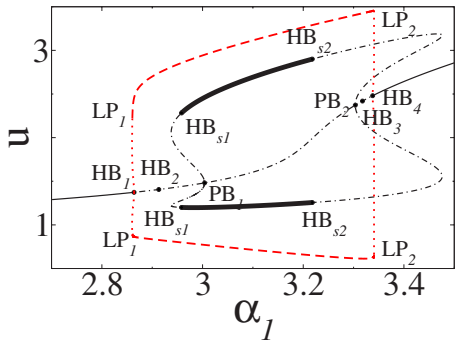

FIG. 4. (Color online) Bifurcation diagram obtained by variation of α_1, to illustrate the OD. The coupling strength is $d=0.01$. Other parameters are the same as in Fig. 2. Thin solid lines denote stable steady state; thick solid lines a stable OD regime; dash-dotted lines unstable steady state; dotted lines unstable limit cycle; and dashed lines stable limit cycle.

systematic qualitative changes in the system. The change of the other parameter α_2 will result in the appearance of identical regimes due to the symmetry of the toggle switch. For each regime we analyze also the influence of the parameters ε and d. The analysis is obtained using the XPPAUT package [36] for a system of two coupled genetic oscillators ($N=2$) to show that already two oscillators provide a large variety of possible regimes.

A. Steady state formation

The OD (Fig. 2) is a result of the symmetry breaking of the steady state in the system through a pitchfork bifurcation (labeled PB_1 in Fig. 4). Thus, the unstable homogeneous steady state splits into two additional branches which gain stability through Hopf bifurcations, denoted as HB_{s1} (HB_{s2}) in Fig. 4. This stabilization occurs for $d>d_{crit}$, which is approximately 0.006 for the set of parameters used here. The inhomogeneous steady state is manifested through two branches of the stable steady state solution, which correspond to two levels of protein concentrations in Figs. 2(a)–2(d). The solution coexists in the α_1 parameter space with different oscillatory solutions, e.g., with the synchronous regime (see Fig. 4). For different values of the parameters there is also coexistence of OD with antiphase oscillations (see Fig. 9 below).

The structure of the stable clusters is different for small and large values of the coupling strength d. When d is subsequently increased, five different states coexist in the given parameter range ($\alpha_1 \epsilon$ [2.76,2.88] and $\alpha_1 \epsilon$ [3.34,3.62]); three of them are stable, and two are unstable (Fig. 5). The pitchfork bifurcation is now shifted, marking the end of the homogenous steady state, which becomes unstable and splits into two separate branches, as discussed previously. Figure 5 also shows the coexistence with the in-phase oscillatory regime, marked with dashed lines.

It is important to note that the Hopf bifurcations HB_{s1} and HB_{s2} give rise also to additional branches of periodic solutions which are unstable and therefore omitted for clarity.

B. Oscillatory regimes

1. In-phase oscillatory regime

The Hopf bifurcations labeled HB_1 and HB_4 in Fig. 6(a) give rise to a branch of periodic orbits, corresponding to a synchronous in-phase solution [see Fig. 3(a)], i.e., there exist synchronous oscillations of the protein concentration over both cells. Figures 6(b) and 6(c) illustrate in more detail the bifurcation structure of the full system when α_1 is subsequently being varied and α_2 is kept fixed. Two subcritical Hopf bifurcations mark the entering and exiting from the in-phase oscillatory regime [HB_1 for $\alpha_1=2.864$ and HB_4 at $\alpha_2=3.338$; Fig. 6(a)–6(c)]. The stable in-phase oscillatory region is determined with two saddle-node bifurcations LP_1 and LP_2. It is important to note that the in-phase oscillations present in the system are stable for any values of d. The periodic branch rising from HB_1 (HB_4) coexists in the same parameter space with the OD clusters, and, as shown further, with the antiphase and the asymmetric oscillatory regimes, thus establishing multistability in the system.

2. Antiphase oscillatory regime

For a small coupling coefficient ($d<0.01$) which depends on the diffusion properties of the cell membrane, stable an-

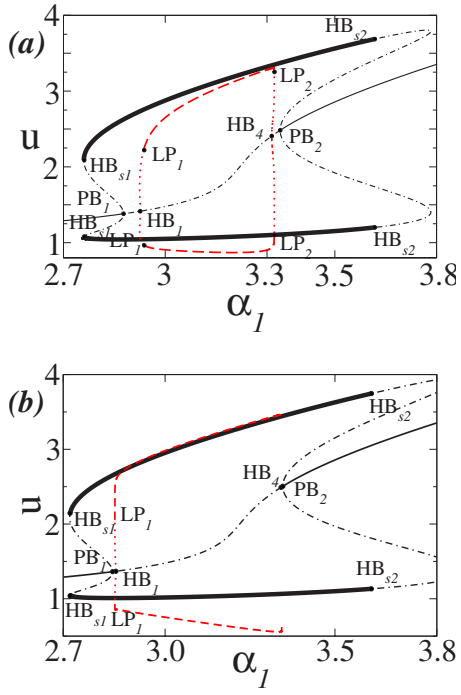

FIG. 5. (Color online) Coexistence of five different states for increased coupling strength $d=0.3$ and $\varepsilon=$(a) 0.05, (b) 0.01. For other parameters see Fig. 2. Coexistence of the OD and the in-phase oscillatory regime is also shown. Thin solid lines denote stable steady state, thick solid lines a stable OD regime, dash-dotted lines unstable steady state, dashed lines stable limit cycle (in-phase regime), and dotted lines unstable limit cycle. Note: Due to the large stiffness of our multidimensional model and the proximity to the bifurcation point, the correct continuation could not be performed with the XPPAUT package. Therefore the branch on Fig. 5(b) is not closed.

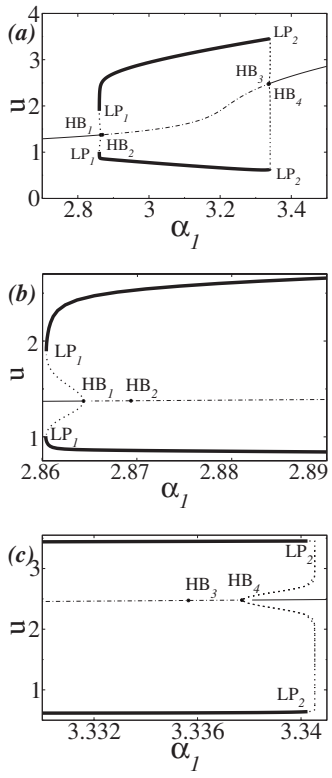

FIG. 6. Formation of oscillatory solution. (a) Bifurcation diagram of the system obtained by variation in α_1 for a fixed value of α_2 (α_2=5) and d=0.001. For other parameters see Fig. 2. (b) Detailed view of HB_1 and HB_2. (c) Detailed view of HB_3 and HB_4. Thin solid lines denote stable steady state, thick solid lines stable limit cycle, dash-dotted lines unstable steady state, and dotted line unstable limit cycle.

tiphase oscillations [see Figs. 3(b) and 3(c)] can be observed. The periodic branch giving rise to the antiphase solution is marked again with two Hopf bifurcations: HB_2 at α_1 =2.869 and HB_3 at α_1=3.336 (Fig. 7).

Stable antiphase oscillations are observed from α_1 =3.224 until α_1=3.290. This solution is stabilized through a saddle-node bifurcation and loses its stability via pitchfork bifurcation (LP_1, PB_2 in Fig. 7). For decreased values of ε,

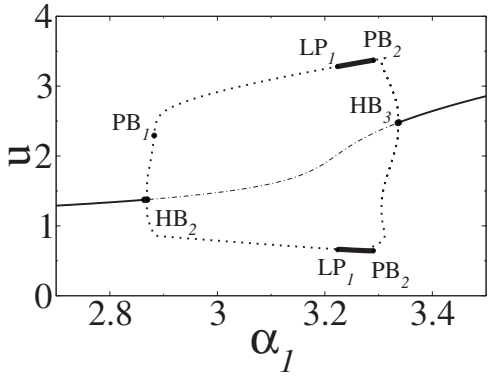

FIG. 7. Bifurcation diagram of the antiphase solution for d =0.001 and other parameters as in Fig. 2. The pitchfork bifurcation marked as PB_1 will be used further in the paper as starting point for the asymmetric solution. For line notations refer to Fig. 6.

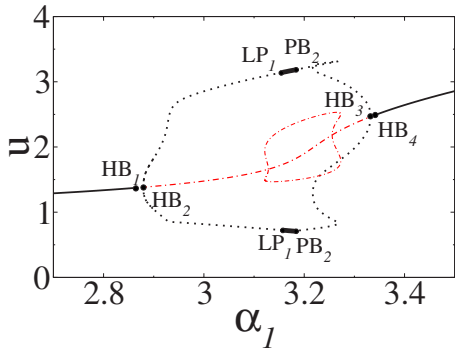

FIG. 8. (Color online) Decreased stability region of the antiphase solution for increased coupling strength d=0.003. Other parameters are the same as in Fig. 2. For line notations refer to Fig. 6.

on the other hand, the region of a stable antiphase regime is significantly increased (results not shown). The behavior of the system, however, is changed when d increases. The complex situation that arises in this case is characterized by a qualitative difference in the particular bifurcation branch (Fig. 8), which results in a subsequent decrease of the stable oscillatory antiphase solution. For some parameter values, the coexistence of antiphase oscillations with stable steady state clusters can be observed (Fig. 9). This important feature of the system of globally coupled genetic relaxation oscillators has not been observed previously for networks constructed from synthetic genetic oscillators or for the system of globally coupled electrochemical oscillators where OD is discussed.

3. Asymmetric oscillatory regime

Another mode of collective behavior in the system of coupled genetic oscillators is characterized by the presence of large and small amplitude oscillations in one attractor, the solution, to which we refer as asymmetric [see Figs. 3(d) and 3(e)]. In this regime, one of the oscillators performs large excursions, while the other one oscillates near the steady state with a small amplitude. The structure of the bifurcation branch which contains this solution is very complex and therefore we demonstrate only the main steps that result in the appearance of a stable asymmetric limit cycle. In particular, for α_1=2.882 a pitchfork bifurcation, labeled as PB_1 in

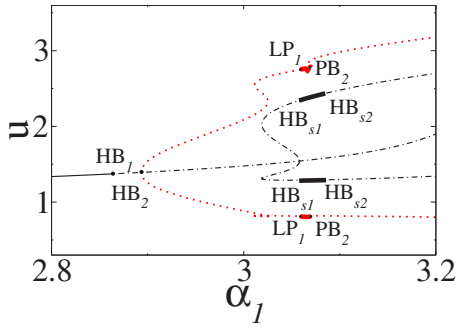

FIG. 9. (Color online) Coexistence of antiphase oscillations (between LP_1 and PB_2) and stable steady state clusters (between HB_{s1} and HB_{s2}) for d=0.006 and other parameters as in Fig. 2.

Fig. 7 [Figs. 10(a) and 10(b)], is found on the bifurcation branch which gives rise to the antiphase oscillations. From this broken symmetry bifurcation point, a secondary unstable bifurcation branch is started [Fig. 10(a)]. In the beginning, this solution has a small degree of asymmetry. The one-parameter continuation for the asymmetric solution moves the bifurcation parameter in the direction of HB_1 (HB_2), approaching the maximum value of u to the unstable steady state. The bifurcation parameter is then shifted to the area of subcritical HB, and the asymmetric regime gains stability in the LP bifurcation which changes the direction of the one-parameter continuation [the stability region is depicted with thick lines in Fig. 10(b) (zoomed region)]. The increase of the bifurcation parameter α_1 further results in a torus bifurcation at $\alpha_1=2.877$ [labeled as TR in Fig. 10(b)], leading to the instability of the regime of asymmetric oscillations. This torus bifurcation ensures the presence of two different incommensurate frequencies. For isolated oscillators ($d=0$) and for $\alpha_1 > \alpha_{HB_1}$, the first frequency is that of a large cycle, and the second one is determined by the eigenvalues of the focus which is unstable. The interaction of these frequencies results in a "beating" behavior, easily seen in Fig. 11(a) where time series of the variables w_i, w_e are plotted. In Fig. 11(b) we show the phase plane (w_i, u_i) where we directly demonstrate how the unfolding of the trajectory from the unstable focus is held from large amplitude oscillations inside the large cycle. The phase point of the large cycle should move faster than that of the small cycle and the successful holding breaks if the larger period decreases when α_1 is increased. This situation is shown in XPPAUT as the torus bifurcation in Fig. 10(b). The distance between the two cycles is not large, which results in the large sensitivity of this regime to external perturbations. Due to the symmetry of the system, this asymmetric solution can be also observed near HB_4.

V. SUMMARY AND OUTLOOK

The presence of multistability and multirhythmicity in synthetic genetic circuits is an important phenomenon from an engineering perspective, since both offer an intriguing potential for numerous biotechnological applications. We have shown in this paper that AI-mediated inhibitory coupling in a system of synthetic genetic relaxation oscillators, functioning through multiple time scales, is a source of multistability and multirhythmicity. Our main result is significantly different from that obtained in studies of coupled circadian oscillators [22–24]; namely, the global and robust in-phase regime reported to be natural in a population of circadian oscillators is a result of the nonrelaxatory oscillations with phase attractive coupling, whereas the presence of multistability in our model is a result of phase repulsive inhibitory coupling and relaxatory dynamics. The presence of global coupling between the oscillators in the system results also in clustering. We have identified many possible modes of collective behavior in this system, distinguishing two types of cluster formation: steady state and oscillatory clusters. Each separate cluster formation is further characterized by a different protein production level, different period of

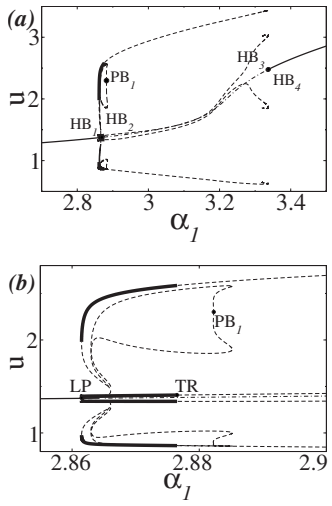

FIG. 10. (a) Bifurcation diagram obtained by variation in α_1. $d=0.001$ and other parameters as in Fig. 2. (b) Detailed view of the region where the stable asymmetric solution exists. Between LP and TR, one oscillator has a large amplitude and the other oscillates with small amplitude. For line notations refer to Fig. 6. Note: The branch on Fig. 10(a) is not closed for the same reasons named in the Fig. 5 caption.

oscillations, or existence of multiple rhythms. In the current set of parameters, the minimal degree of cooperativity has been used (all Hill coefficients equal 2). We suggest that an increase of stability of nontrivial limit cycles over wider parameter ranges may be associated with the use of other elements with large Hill coefficients.

The dynamical richness observed in this particular model can be considered as a significant advantage for a multitude of applications (biosensors, programming genetic units, etc.). In this paper we have presented a minimal manifestation of

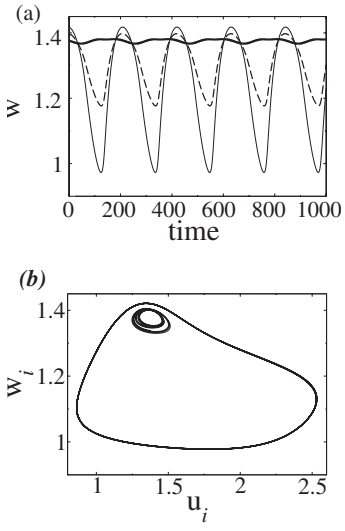

FIG. 11. (a) Time series for two oscillators in the asymmetric regime. $d=0.001$ and other parameters correspond to Fig. 2. The thick solid line represents w_1, thin solid line w_2, and dashed line w_e. (b) Phase portrait of the two coupled oscillators in the asymmetric regime. Small cycle corresponds to one and large cycle to the second oscillator.

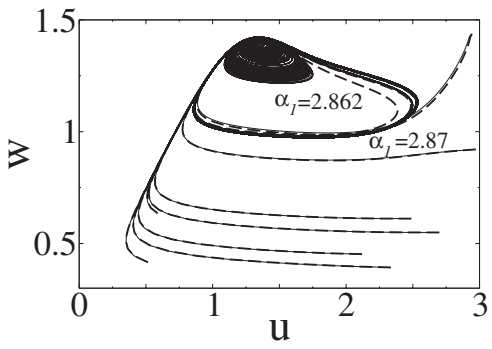

FIG. 12. Large amplitude changes due to the variation of the α_1 parameter values for system of $N=8$ oscillators.

multistability because identical elements have been considered. It is well known that the set of possible regimes is enlarged if more realistic heterogeneity is taken into account. Moreover, for relaxation oscillators chosen not far from a Hopf bifurcation, the in-phase regime may become unstable due to the heterogeneity of the elements.

It has been reported that multistability is a main mechanism for memory storage and temporal pattern recognition in artificial and natural neural networks [37]. Moreover, the effect of multistability is also used to create an electrically addressable passive device of organic molecules [38] for registration, storage, and processing of information. Therefore, it is logical to assume that the ability of the genetic circuits to display multistability opens the possibility for construction of new-era computational devices, based on genetic and DNA computing. In addition, it is very important to note that the presence of different periods for different oscillator distributions in every regime reported here opens the possibility for a resonant behavior of the system on multitude frequencies. This result can be important, e.g., for the construction of genetic networks driven by a periodic signal [4] coupled with cell cycle regulation. It also means that different synchronization regions can be obtained for different external frequencies, an effect which can have impact in cancer chronotherapy or cell cycle regulation. We emphasize the generality of these results, although derived for this particular model of genetic network, since no special properties of the given system were used to obtain the appearance of multistability, multirhythmicity, and clustering.

It is also important to mention that the existence of the asymmetric regime enables the system of globally coupled genetic relaxation oscillators to exhibit very sensitive amplitude changes due to the variation in the α_1 parameter values (Fig. 12). Phenomenologically, this regime is very similar to localized patterns which have in the background a Canard behavior near the supercritical Hopf bifurcation [39]. We assume that asymmetrical regimes near subcritical bifurcations are more robust than asymmetrical regimes near supercritical Hopf bifurcations, under the same time scale separation. The asymmetrical regime presented here opens the possibility for the construction of very compact and precise biosensors with increased sensitivity.

ACKNOWLEDGMENTS

A.K. acknowledges the International Max Planck Research School on Biomimetic Systems, E.V the Program "Radiofizika" of Russian Academy of Sciences, Grant No. RFBR 05-02-16518-, and the International graduate school "Computational Neuroscience of Behavioral and Cognitive Dynamics," A.Z. the Volkswagen-Stiftung, CESCA-CEPBA (HPC-Europa Transnational Access program), and J.K. the EU through the Network of Excellence BioSim, Contract No. LSHB-CT-2004-005137. The authors thank A. Kuznetsov for fruitful discussions.

[1] S. L. Garfinkel, Technol. Rev. **3**, 70 (2000).
[2] T. S. Gardner, C. R. Cantor, and J. J. Collins, Nature (London) **403**, 339 (2000).
[3] M. B. Elowitz and S. Leibler, Nature (London) **403**, 335 (2000).
[4] J. Hasty, F. Isaacs, M. Dolnik, D. McMillen, and J. J. Collins, Chaos **11**, 207 (2001).
[5] D. McMillen, N. Kopell, J. Hasty, and J. J. Collins, Proc. Natl. Acad. Sci. U.S.A. **99**, 679 (2002).
[6] R. Weiss, S. Basu, S. Hooshangi, A. Kalmbach, D. Karig, R. Mehreja, and L. Netravali, Natural Comput. **2**, 47 (2003).
[7] J. García-Ojalvo, M. Elowitz, and S. Strogatz, Proc. Natl. Acad. Sci. U.S.A. **101**, 10955 (2004).
[8] A. Kuznetsov, M. Kern, and N. Kopell, SIAM J. Appl. Math. **65**, 392 (2005).
[9] R. Wang and L. Chen, J. Biol. Rhythms **20**, 257 (2005).
[10] L. Chen, R. Wang, T. Zhou, and K. Aihara, Bioinformatics **21**, 2722 (2005).
[11] A. Mustafin and E. Volkov, Biol. Cybern. **49**, 149 (1984).
[12] E. Volkov and M. Stolyarov, Phys. Lett. A **159**, 61 (1991).
[13] E. Volkov and M. Stolyarov, Biol. Cybern. **71**, 451 (1994).
[14] N. Kopell and D. J. Somers, J. Math. Biol. **33**, 261 (1995).
[15] D. Ruwisch, M. Bode, D. Volkov, and E. Volkov, Int. J. Bifurcation Chaos Appl. Sci. Eng. **9**, 1969 (1999).
[16] O. Decroly and A. Goldbeter, Proc. Natl. Acad. Sci. U.S.A. **79**, 6917 (1982).
[17] T. Haberichter, M. Marhl, and R. Heinrich, Biophys. Chem. **90**, 17 (2001).
[18] K. Tsaneva-Atanasova, C. L. Zimliki, R. Bertram, and A. Sherman, Biophys. J. **90**, 1 (2006).
[19] G. Ullah, P. Jung, and A. H. Cornell-Bell, Cell Calcium **39**, 197 (2006).
[20] J. Wolf and R. Heinrich, Biochem. J. **345**, 321 (2000).
[21] V. In, A. Kho, J. D. Neff, A. Palacios, P. Longhini, and B. K. Meadows, Phys. Rev. Lett. **91**, 244101 (2003).
[22] D. Gonze, S. Bernard, C. Waltermann, A. Kramer, and H. Herzel, Biophys. J. **89**, 120 (2005).
[23] H. Kunz and P. Achermann, J. Theor. Biol. **224**, 63 (2003).
[24] H. R. Ueda, K. Hirose, and M. Iino, J. Theor. Biol. **216**, 501 (2002).
[25] K. Kaneko, Physica D **63**, 424 (1990).
[26] D. Golomb, D. Hansel, B. Shraiman, and H. Sompolinsky,

Phys. Rev. A **45**, 3516 (1992).
[27] K. Okuda, Physica D **63**, 424 (1993).
[28] K. Miyakawa and K. Yamada, Physica D **151**, 217 (2001).
[29] I. Z. Kiss and J. L. Hudson, Chaos **13**, 999 (2003).
[30] W. Wang, I. Z. Kiss, and J. L. Hudson, Phys. Rev. Lett. **86**, 4954 (2001).
[31] H. Kobayashi, M. Kaern, M. Araki, K. Chung, T. Gardner, C. Cantor, and J. J. Collins, Proc. Natl. Acad. Sci. U.S.A. **101**, 8414 (2004).
[32] C. Fuqua and P. E. Greenberg, Nat. Rev. Mol. Cell Biol. **3**, 685 (2002).
[33] I. Prigogine and R. Lefever, J. Chem. Phys. **48**, 1695 (1968).
[34] K. Bar-Eli, Physica D **14**, 242 (1985).
[35] Y. Zhai, I. Z. Kiss, and J. L. Hudson, Phys. Rev. E **69**, 026208 (2004).
[36] B. Ermentrout, *Simulating, Analyzing, and Animating Dynamical Systems: A Guide to Xppaut for Researchers and Students (Software, Environments, Tools)* (SIAM Press, Philadelphia, PA, 2002).
[37] J. Foss, A. Longtin, B. Mensour, and J. Milton, Phys. Rev. Lett. **76**, 708 (1996).
[38] H. Gudesen, P. Nordal, and G. Leistad, U.S. Patent No. 6055180 (1999).
[39] H. G. Rotstein and R. Kuske, Physica D **215**, 46 (2006).